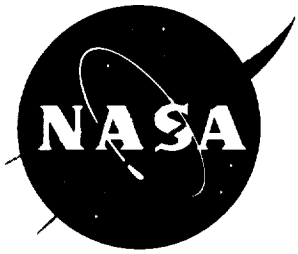

NASA Technical Paper 3560

A Conceptual Design for the Attitude Control and Determination System for the Magnetosphere Imager Spacecraft

M.E. Polites and C.K. Carrington

May 1995

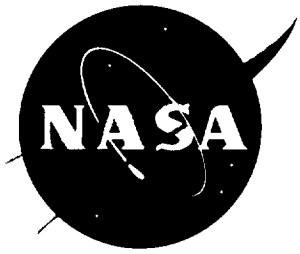

NASA Technical Paper 3560

A Conceptual Design for the Attitude Control and Determination System for the Magnetosphere Imager Spacecraft

M.E. Polites and C.K. Carrington
Marshall Space Flight Center • MSFC, Alabama

National Aeronautics and Space Administration
Marshall Space Flight Center • MSFC, Alabama 35812

May 1995

TABLE OF CONTENTS

LIST OF ILLUSTRATIONS

LIST OF ILLUSTRATIONS (CONCLUDED)

LIST OF TABLES

TECHNICAL PAPER

A CONCEPTUAL DESIGN FOR THE ATTITUDE CONTROL AND DETERMINATION SYSTEM FOR THE MAGNETOSPHERE IMAGER SPACECRAFT

I. INTRODUCTION

The Magnetosphere Imager (MI) is a faster-better-cheaper type spacecraft that has been proposed for launch by NASA in 1999 into a polar Earth orbit. The total cost of the spacecraft and all associated expenses has been specified by NASA Headquarters to be $80 million or less, not counting the cost of the launch vehicle. Recently, an MI conceptual design study was performed at NASA's Marshall Space Flight Center. This paper presents the resulting conceptual design for the spacecraft's attitude control and determination (ACAD) system. Leading up to this, section II gives a brief overview of the MI mission. Then, section III defines the ACAD requirements for the spacecraft. In section IV, the conceptual design for the ACAD system is presented. Section V presents analysis and simulation results to date which support the soundness of the ACAD system design approach. Concluding remarks are made in section VI.

II. MISSION OVERVIEW

The MI spacecraft is projected for launch in 1999 from the Western Test Range at Vandenberg Air Force Base, CA. The launch vehicle is the Taurus-S, a medium-light class expendable launch vehicle built by Orbital Sciences Corporation (OSC). It will place the 300 kg, 1.3 m diameter × 1.3 m high cylindrical spacecraft into a highly elliptical polar orbit with a 44,650 km (7 R_e) apogee and a 4,800 km (0.75 R_e) perigee. Its initial argument of perigee has been selected to be 270°, which places the initial orbit perigee over the South Pole. The argument of perigee will precess about 41° over the 2-year mission (see fig. 1). The longitude of the ascending node at the start of the mission will be chosen to give an initial beta angle (i.e., the angle between the sunline and the orbit plane) that is close to 0°. Because of the polar orbit, the longitude of the ascending node will not change with time, but the beta angle will vary between ±66.5° over the 2-year mission. The orbit period is 15 h 10 min.

Throughout the course of the mission, three scientific instruments on the spacecraft will collect data and store it on an onboard solid state recorder. These data will be periodically telemetered to the ground via NASA's Deep Space Network (DSN) and will be used to generate images of the Earth's magnetosphere, the region formed by the interaction of the solar wind with the Earth's magnetic field. These images will allow scientists to better understand the influence of the Sun on the Earth's environment.

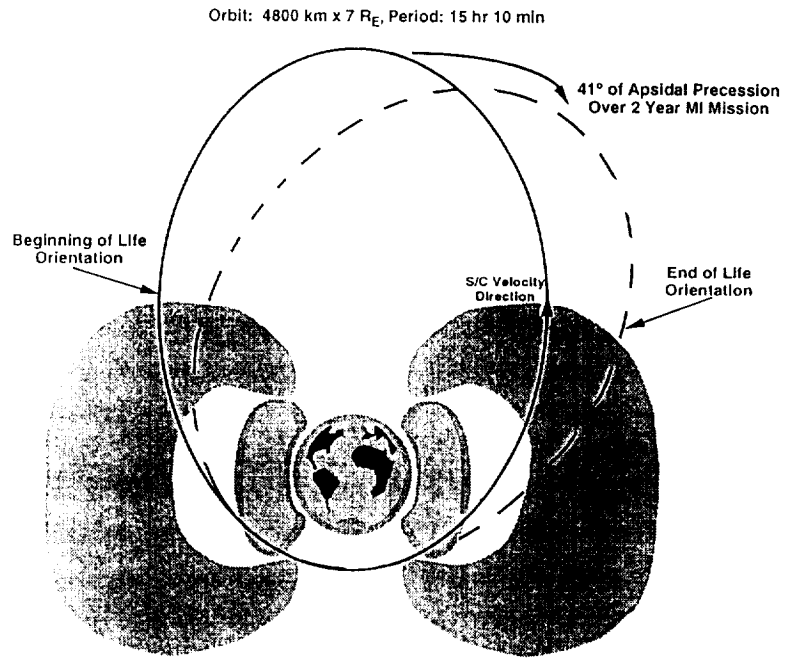

Figure 1. Spacecraft orbit at the beginning and end of the MI mission.

III. ACAD REQUIREMENTS

The three MI science instruments are the High Plasma Imager (HPI) with its two high energy heads and one low energy head, the Plasmasphere Imager (PI), and the Far Ultraviolet (FUV) Imager. The location of these instruments in the spacecraft is shown in figure 2. Body mounted solar panels are mounted all around the spacecraft for electrical power, but these are not shown in the figure. For these science instruments to obtain useful science data, the spacecraft must spin about a body fixed axis that is within 0.025° of the spacecraft's geometric centerline, at a spin rate in the range of 10±5 rpm, and the spin axis must be kept closely aligned with the orbit normal. How close depends on the science instrument, as shown in table 1. Other science instrument ACAD characteristics and requirements are shown in this table. From these and the other science instrument requirements identified, the MI ACAD system derived requirements can be established; these are shown in figure 3.

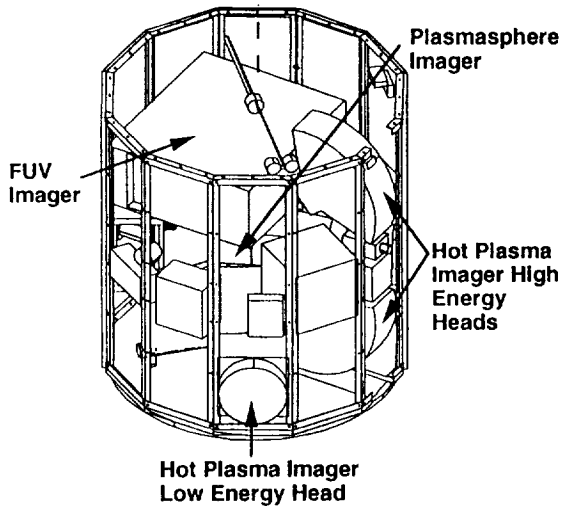

Figure 2. Location of the science instruments.

Table 1. Science instrument ACAD requirements.

Science Instrument	Field of View	Required Accuracy of Orienting Spin Axis wrt Orbit Normal	Allowable Spin Axis Drift Over Any 60 s Period	Required Knowledge of SI Attitude on Ground
Hot Plasma Imager (HPI)	4 pi steradians	5°	0.5°	0.5°
Plasmasphere Imager (PI)	135°×360°	1°	0.5°	0.5°
FUV Imager	40°×360°	1°	0.025°	0.025°

- Spin Spacecraft at 10±5 rpm
- Keep Spin Axis:
  - Within 1° of Orbit Normal
  - Drift <0.025° Over Any 60 s Period
- Keep Axis of Maximum Principal Moment of Inertia <0.025° of Spacecraft Centerline
- Reconstruct Science Instrument Attitudes on Ground to:
  - <0.5° for Hot Plasma Imager and Plasmasphere Imager
  - <0.025° for FUV Imager

Figure 3. ACAD system derived requirements.

IV. ACAD SYSTEM CONCEPTUAL DESIGN

The derived ACAD requirements in figure 3 and the requirement to make MI a smaller-cheaper-faster spacecraft drives the MI to be a spin stabilized spacecraft with an ACAD system that is simple and highly passive. A hardware block diagram for the proposed ACAD system is shown in figure 4. A component equipment list is given in table 2. A functional mounting arrangement for these components is shown in figure 5. Of course, variations to this are possible. A detailed description of this system, how it satisfies the requirements in figure 3, and its underlying design philosophy are given below. Refer to figures 4 and 5 and table 2 in this description.

For the MI to be spin stabilized and to spin about a body-fixed axis that is within 0.025° of the spacecraft's geometric centerline, several things are required. First, the axis of maximum principal moment-of-inertia needs to be accurately aligned with the geometric centerline prior to launch. Hence, all of the spacecraft hardware needs to be mounted with this in mind. After all of the hardware is mounted, a spin balance machine is needed to determine where small trim masses can be

strategically placed on the spacecraft to further reduce the principal axis offset angle. The process of spin balancing the spacecraft needs to be done during the hardware integration phase and at the launch site to insure that the offset angle is as small as possible at launch. A residual offset angle below 0.25° should be readily achievable with spin balancing. Secondly, the spacecraft needs an onboard mass balance system that can be certain to trim the offset angle to within 0.025° in orbit. The onboard system is described by figures 4 and 5 and table 2. Thirdly, the ratios of the maximum principal moment-of-inertia to the intermediate and the minimum should be 1.07 or more at launch, but the design goal should be 1.2 or more.

Although not required, it is desirable to have the minimum and the intermediate principal moments-of-inertia numerically close to one another, to within about 1 kg-m^2, in order to minimize the gravity torque along the spacecraft spin axis. It is also desirable to have the center-of-mass close to the geometric center, to within about 2 cm, in order to minimize the solar radiation torque on the spacecraft. Preliminary mass properties for the MI, with no contingency mass added, reveal the following: when 3.1 kg and 1.3 kg trim masses are properly mounted on the spacecraft, the principal moments-of-inertia become 64.2 kg-m^2, 60.2 kg-m^2, and 60.0 kg-m^2; the axis of maximum principal moment-of-inertia becomes aligned with the spacecraft's geometric centerline; the total spacecraft mass becomes 224 kg; and the center-of-mass is within 1 cm of the spacecraft's geometric center. These mass properties satisfy the stated requirements and goals; however, as the spacecraft design matures, attempts should be made to try to increase the ratios between the maximum principal moment-of-inertia and the other two.

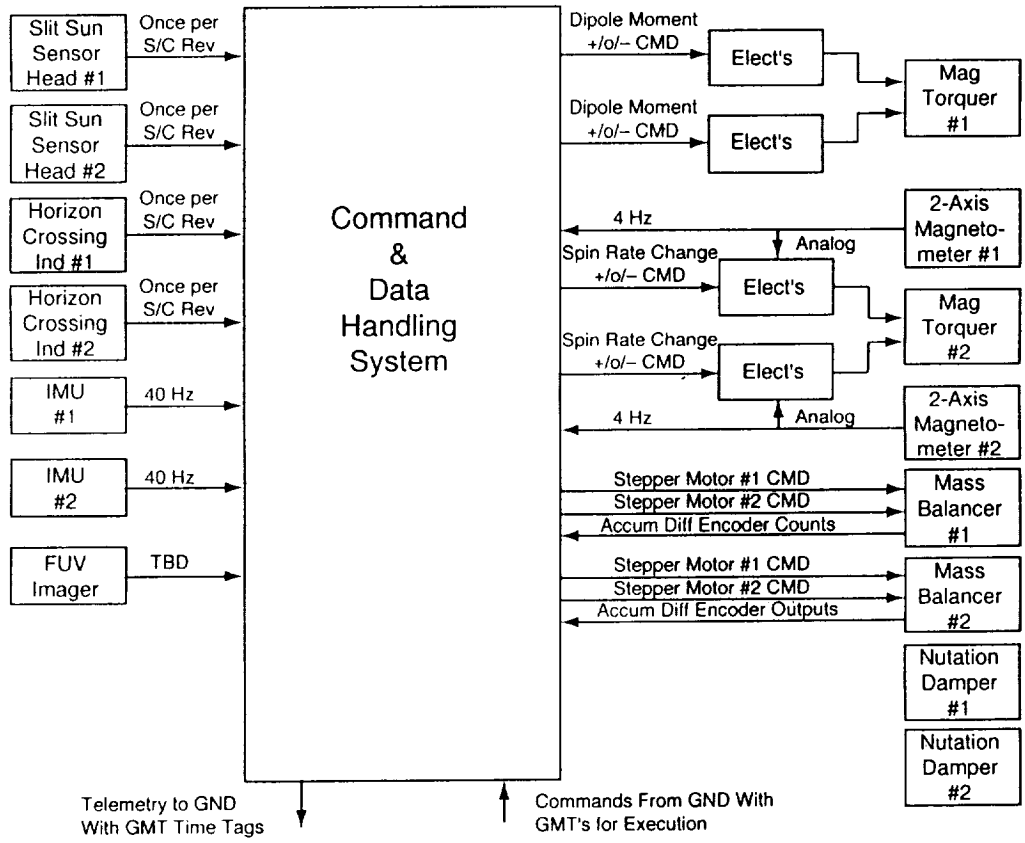

Figure 4. ACAD system hardware block diagram.

Table 2. ACAD system equipment list.

Component	Vendor and Model Number	Number of Units on S/C	Range	Accuracy	Size	Mass	Power	Design Status
Digital sun sensor for spinning S/C	Adcole 18810	1 assembly with 2 heads	±64° linear FOV per head	LSB = 0.25°	6.6×3.3×2.5 cm per head and 10.4×5.8×9.4 cm for elect	0.95 kg for complete assembly	0.4 W for complete assembly	Flight proven
Horizon crossing indicator	Barnes 13-210B	2	±5.7° lin. FOV per unit at apogee, ±24° at perigee	0.1° (3-sigma)	7.7×10.5×20.2 cm per unit	0.74 kg per unit	1.5 W for one unit	Flight proven
IMU	Litton LN-200	2	±1,000°/s for rate and ±40 g for acc	Scale factor error = 50 ppm for rate and 300 ppm for acc	Each IMU is 8.9 cm dia and 7.9 cm high	0.72 kg per IMU	10 W avg for one IMU	Flown on Clementine in 1994
Two-axis magnetometer	Ithaco IM-102	2	±0.6 gauss	Noise = 0.05 milligauss (rms)	11.4×5.8×2.5 cm per sensor	0.22 kg per sensor	0.04 W for one sensor	Off the shelf
Magnetic torquer	Ithaco TR230UPR	2 with redundant windings	Command ±200 a-m^2 or 0 a-m^2	±10 percent of command	Each torquer is 3.0 cm dia and 91.4 cm long	4.4 kg per torquer	3.8 W per torquer when on and <<1 W avg	Off the shelf
Nutation damper	URENCO	2	Reduces spin axis wobble from 1° to 0.025° in 1.2 h		Each damper is 47×24×12 cm	0.54 kg per damper	None	Flown on ESA's COS-B S/C in 1975
Mass balancer	Build in-house	2	Each unit has a 1 kg mass that can move ±0.5 m	Min change in mass position is ±2 mm	Each unit is 100×20×10 cm	3 kg per unit	2 W max and <<1 W avg	Long flight heritage

ACAD Totals: Mass = 20.2 kg, Power = 12 W avg

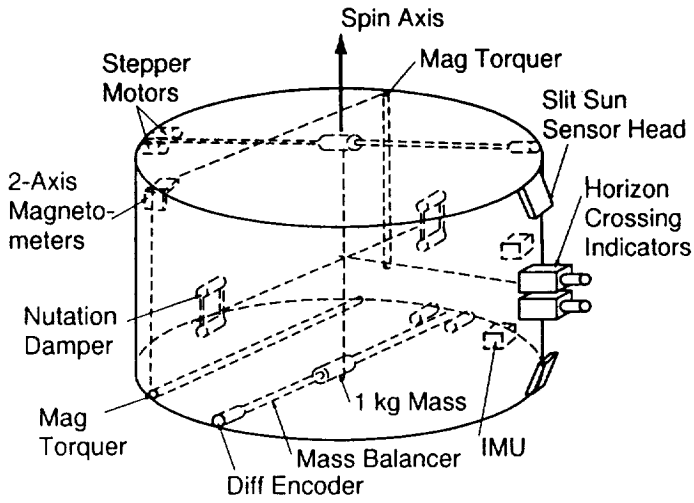

Figure 5. A functional mounting arrangement for the ACAD components.

To achieve the desired spin rate, the last stage of the Taurus-S is utilized. After orbit insertion and prior to separation, it can position the spacecraft's geometric centerline close to the orbit normal, to within 2° according to estimates by OSC engineers. Then, it can spin the spacecraft down to the desired 10 rpm. OSC indicates that the last stage with the spacecraft will probably be spin stabilized at 30 rpm for the apogee burn that puts the spacecraft in the final desired orbit. At separation, the tip-off rates should be 3°/s or less, according to OSC.

Upon separation, redundant meridially mounted passive nutation dampers can damp the spin axis wobble resulting from the tip-off rates to less than 0.025° in approximately 2 h (see table 2 and section V). Then, the spacecraft should be spinning about its axis of maximum principal moment-of-inertia at a spin rate of approximately 10 rpm. After several days of spacecraft outgassing, one of the inertial measurement units (IMU's) can be powered up. Then, the onboard Command and Data Handling System (CDMS) can begin reading the IMU rate gyro and accelerometer outputs, time tagging them with Greenwich Mean Time (GMT), and storing this information on the onboard solid state tape recorder, every 0.025 s. Once per orbit, this stored data will be telemetered to ground.

With this data, the ground can determine the angle between the axis of maximum principal moment-of-inertia and the spacecraft geometric centerline. Stepper motor commands to the mass balance system that should reduce this angle to less than 0.025° can also be computed. These commands can be uplinked to spacecraft along with the desired GMT for execution. This process can be repeated until the angle is less than 0.025°.

Now one of the redundant horizon crossing indicators and the appropriate slit Sun sensor head can be powered up and their outputs, every spacecraft revolution, time tagged and stored in the onboard solid state recorder. Once per orbit, this data can be telemetered to the ground. Based on this information and the spacecraft's orbit ephemeris, accurately determined by ground tracking using NASA's DSN or the Air Force's NORAD tracking system, the angle between the spacecraft's spin axis and the orbit normal can be determined. If this is more than the required 1°, the two onboard two-axis magnetometers can be powered up and their outputs, every 0.25 s, time tagged and stored in the onboard recorder. This data can be telemetered to the ground once per orbit. Using it, the horizon crossing indicator data, the slit Sun sensor data, the IMU rate gyro data, and the orbit ephemeris, the ground can determine the GMT's around orbit perigee when the onboard magnetic torquer, that is aligned with the spacecraft spin axis, should be turned on and off, and what its

polarity should be in order to move the spacecraft spin axis to within 1° of the orbit normal. The left hand vector diagram in figure 6 helps to illustrate this. The commands and the GMT's to accomplish this can then be uplinked to the spacecraft. Once the onboard commands have been executed, the spacecraft spin axis should lie within the required 1° of the orbit normal. If not, the process can be repeated until the requirement is satisfied. An alternative to using the magnetometer data in this procedure is to use a ground-based model for the Earth's magnetic field. This is a back-up approach in the event the magnetometers fail.

If the rate gyro measurements show the spacecraft spin rate is not in the range of 10±5 rpm, then corrections to it are required. To make these, the ground uplinks the commands that turn on one of the two-axis magnetometers and the electronics for the magnetic torquer that is normal to the spacecraft spin axis. This simple system with analog electronics logic uses the polarity of one axis of the magnetometer to switch the polarity of the magnetic torquer dipole moment in order to spin the spacecraft up or down. The right hand vector diagram in figure 6 helps to illustrate the basic concept. By this technique, the spin rate can be affected about 0.5 rpm per orbit. The ground also needs to uplink the command that tells the system whether to spin up or spin down the spacecraft and the GMT's to start and stop this process each orbit. There is about an hour each orbit when the Earth's magnetic field is strong enough to be useful. This is when its magnitude is between 0.05 and 0.1 gauss near perigee, as figures 7 and 8 show.[1]

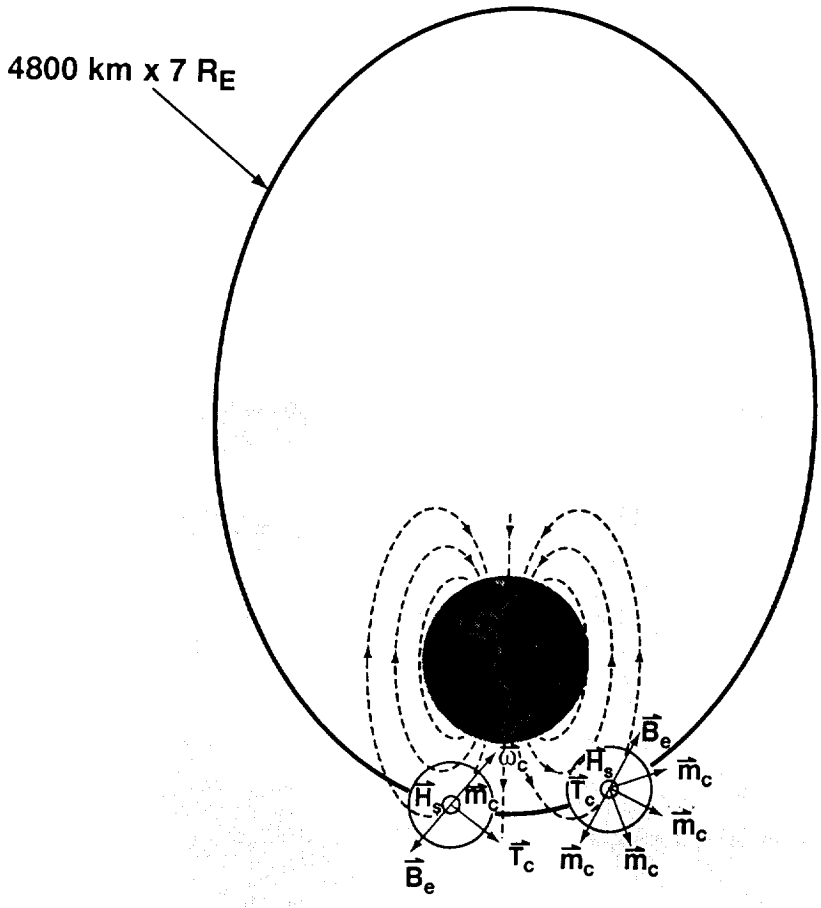

Figure 6. Magnetic control torques for changing the spin axis orientation and spin rate.

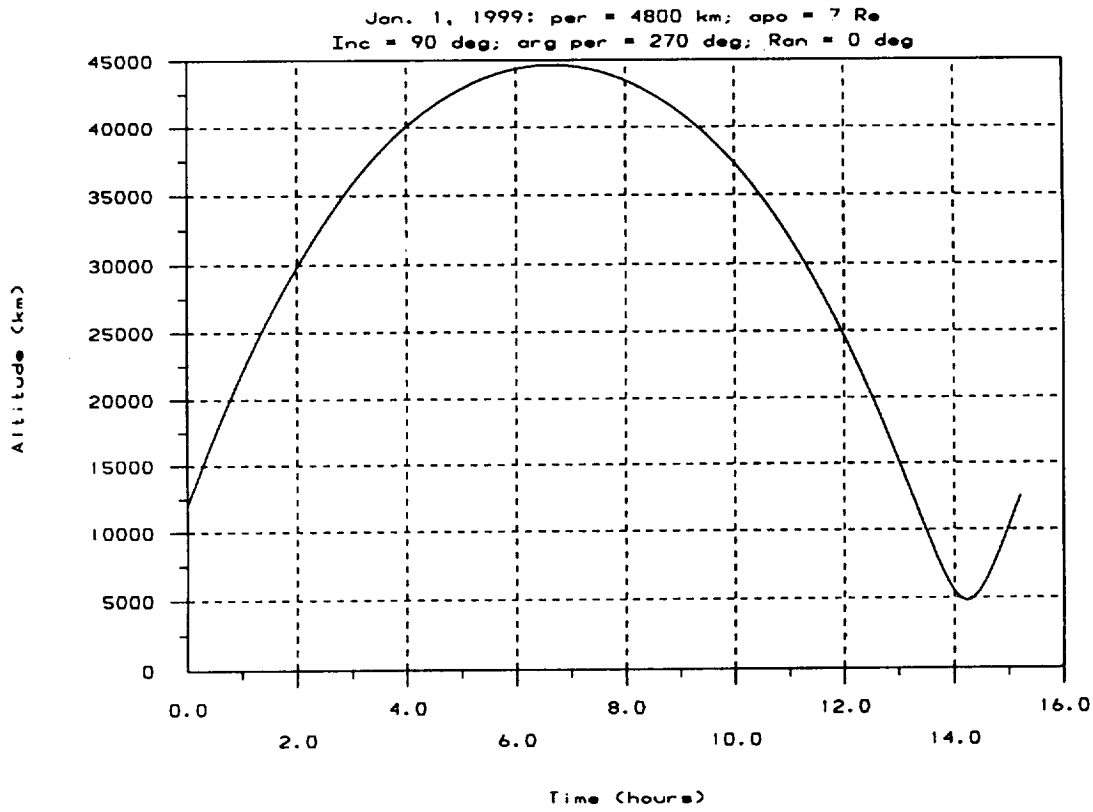

Figure 7. Altitude around the MI orbit.

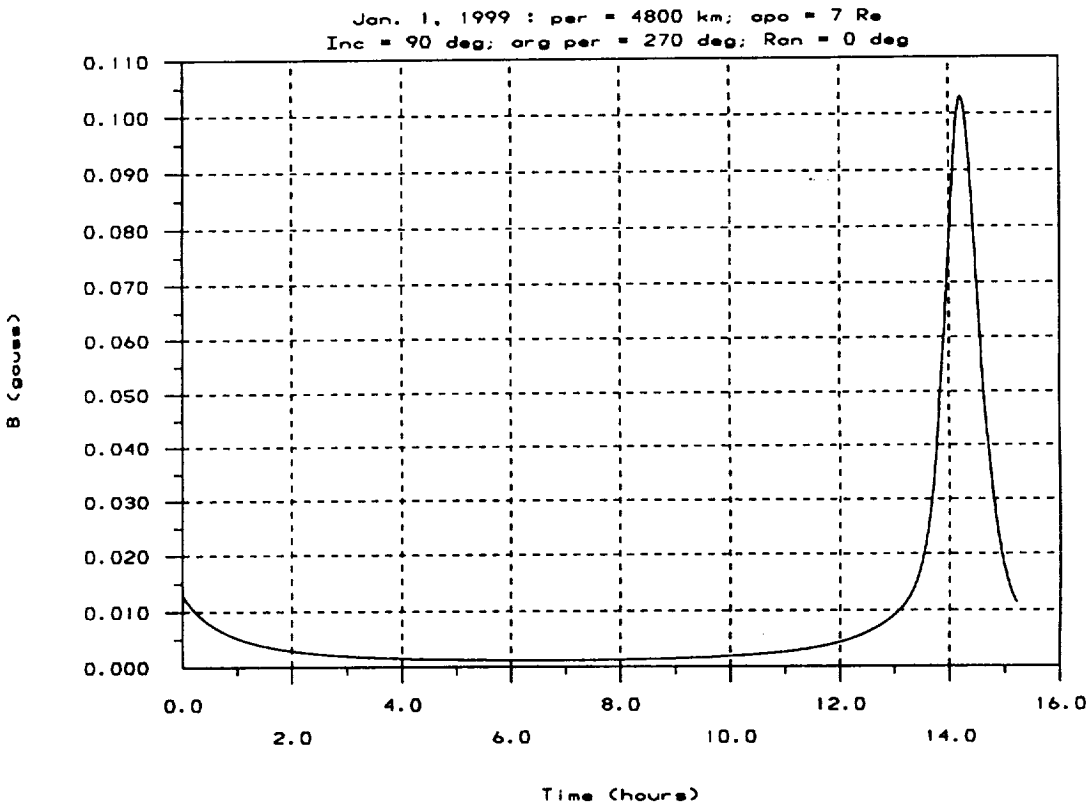

Figure 8. Earth's magnetic field strength around the MI orbit.

The HPI and the PI instruments can now be powered up and their outputs time tagged and stored in the onboard solid state recorder. Again, once per orbit this data can be telemetered to the ground. The ground can use the horizon crossing indicator, the slit Sun sensor, and the IMU rate gyro measurements to reconstruct the attitudes of the HPI heads and the PI to the required 0.5° accuracy.

Now, the FUV Imager can be powered up and its outputs time tagged with GMT and stored in the onboard recorder. Again, once per orbit this data can be telemetered to the ground. It is assumed that the FUV Imager can function like an ultraviolet (UV) star tracker to detect and accurately measure UV stars in its field-of-view (FOV) down to 3 M_V. These measured stars will be used in conjunction with the IMU rate gyro outputs to reconstruct the FUV Imager attitude to the required 0.025° accuracy. The FUV Imager must be able to detect and accurately measure UV stars down to 3 M_V, in order to guarantee having some suitable stars in its FOV each spacecraft rotation, assuming an arbitrary launch date. Figures 9 to 11 illustrate this.[2] If not, then it will be necessary to constrain the launch window. If the FUV Imager output does not function as a UV star tracker, then redundant slit star trackers will need to be added to the ACAD system.

The baselined IMU is attractive because of its low power, low mass, and adequate performance; however, it is nonradiation hardened. If single event upsets (SEU's) turn out to be a frequent occurrence and power is available, both IMU's can be powered up and the rate gyro outputs from the second can be stored in the onboard recorder in place of the accelerometer outputs from the first. Now, the chance of an SEU in both IMU's, in the same orbit, should be small. Hence, the rate gyros measurements from one IMU or the other should be good at all times every orbit. If an SEU occurs in a given IMU, the ground can uplink the command to recycle power to it, which should properly reinitialize it. If there is still a problem with this approach or there is not enough power for the second IMU, then a backup procedure is to uplink a set of commands to recycle power to the appropriate IMU at GMT's spaced 1 h apart. If the SEU's are occurring about once per orbit, then the rate gyro measurements would be bad for only 1 h or less each orbit.

With time, the orientation of the orbit plane with respect to the Sun line will change significantly. This necessitates periodically switching off one Sun sensor head and switching on the other, since the linear FOV of each is 128°. This needs to be done about once every 6 months. When to switch will be known well in advance and poses no problems whatsoever for the ground.

Over a period of time, the orientation of the spacecraft spin axis will drift relative to the orbit normal because of the disturbance torque caused by solar radiation pressure. See table 3 for estimates of the MI disturbance torques, as well as the control torques. The solar radiation torque is a maximum when the beta angle is 45° and a minimum when the beta angle is zero.[3] This assumes the spacecraft spin axis is aligned with the orbit normal. Consequently, the orientation of the spin axis will need to be adjusted periodically using the method described previously. The frequency of this adjustment should be somewhere between once a week and once a month, depending on the beta angle.

The spacecraft spin rate decay is expected to be only about 0.5 rpm over 2 years, which follows from table 3[4–6] and the simulation results in section V. However, if this prediction is wrong and the spacecraft spins down faster, then the scheme previously described for adjusting the spin rate can be utilized periodically.

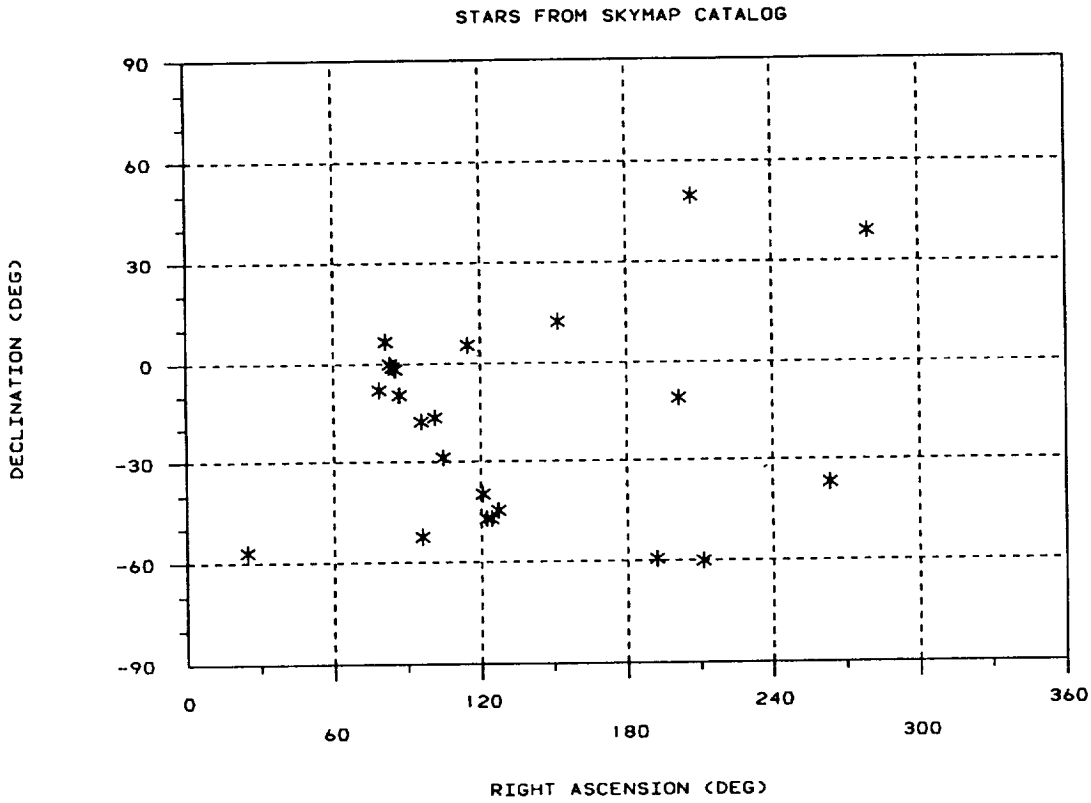

Figure 9. All UV stars brighter than +1 M_V.

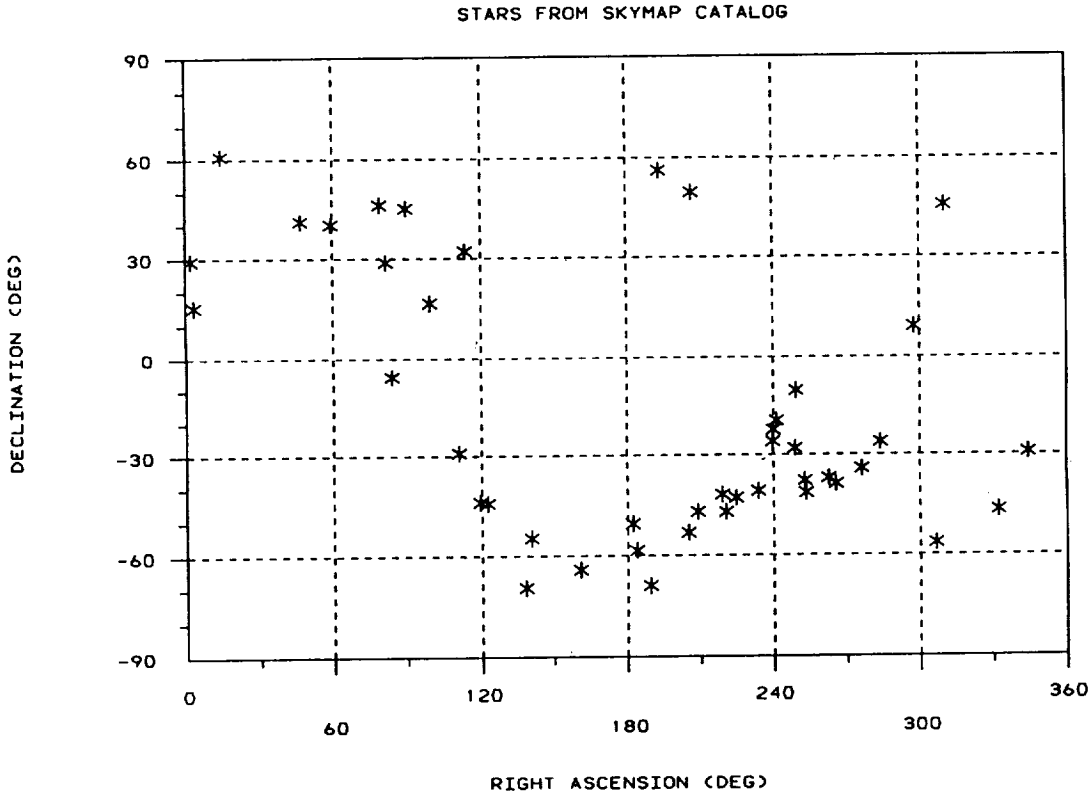

Figure 10. All UV stars between +1 and +2 M_V.

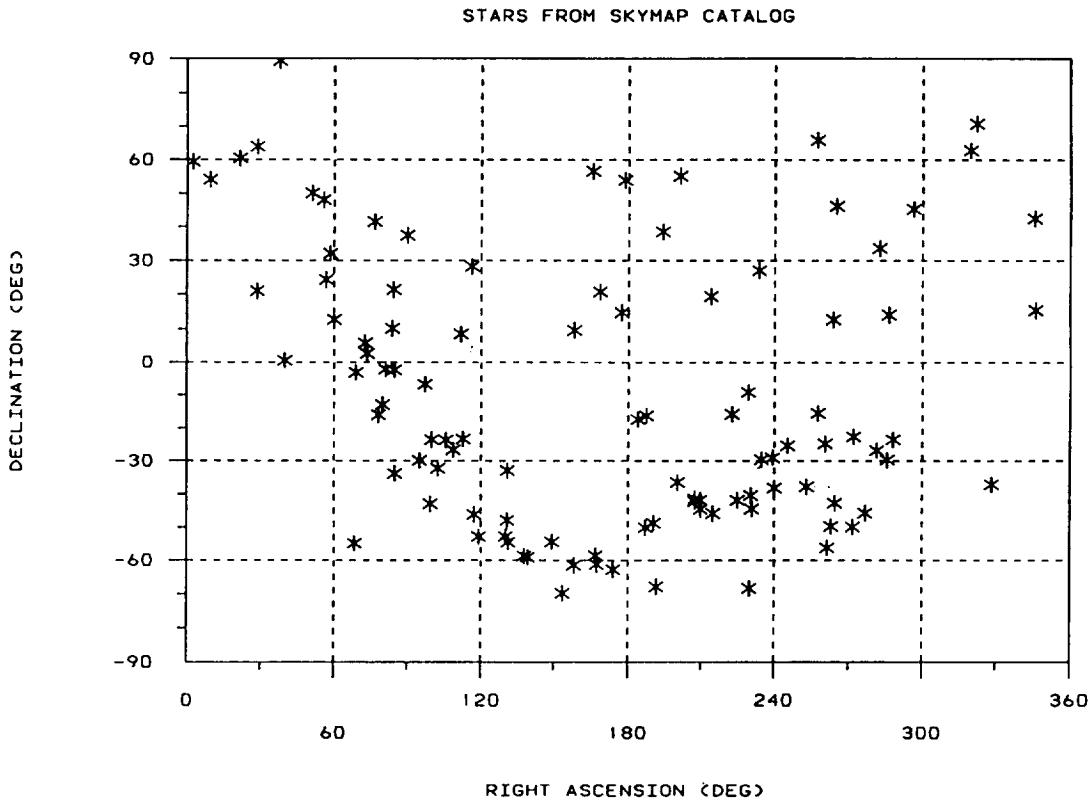

Figure 11. All UV stars between +2 and +3 M_v.

Table 3. Torques on MI.

Torque	Type	Maximum Value	Effect
Solar Radiation Pressure	Environmental Disturbance Torque	1.6×10^{-6} N-m	Causes Spin Axis to Drift 1° in 1 to 4 Weeks
Drag Torque from Eddy Current Losses in Spacecraft Aluminum Structure	Environmental Disturbance Torque	0.9×10^{-6} N-m	Reduces Spin Rate 0.5 rpm in 2 Years
Aerodynamic	Environmental Disturbance Torque	$< 10^{-8}$ N-m	Negligible
Gravity Gradient	Passive Environmental Control Torque	3.4×10^{-6} N-m	Aligns Spin Axis With Orbit Normal
Magnetic Torque for Reorienting Spin Axis	Commanded Control Torque	$2{,}000\times10^{-6}$ N-m in 0.1 Gauss Field at Perigee	Reorients Spin Axis 1° in 13 Min
Magnetic Torque for Spin Rate Correction	Commanded Control Torque	$2{,}000\times10^{-6}$ N-m in 0.1 Gauss Field at Perigee	Changes Spin Rate 0.5 rpm per Orbit
Nutation Dampers' Viscous Friction Torque	Passive Control Torque		Reduces Spin Axis Wobble from 1° to 0.025° in 1.2 h.

V. ACAD SYSTEM ANALYSIS AND SIMULATION RESULTS

The MI spacecraft uses the mass balance system to align the axis of maximum principal moment-of-inertia with the spacecraft geometric centerline. Without a mechanism for energy dissipation, the principal axis would precess about the angular momentum vector, as shown in figure 12. The nutation dampers remove this spin axis wobble and align the principal axis with the angular momentum vector. The angular momentum vector nominally points along the orbit normal, but will be perturbed by the environmental disturbances. The magnetic torquer oriented along the spacecraft spin axis provides a control torque to realign the angular momentum vector with the orbit normal.

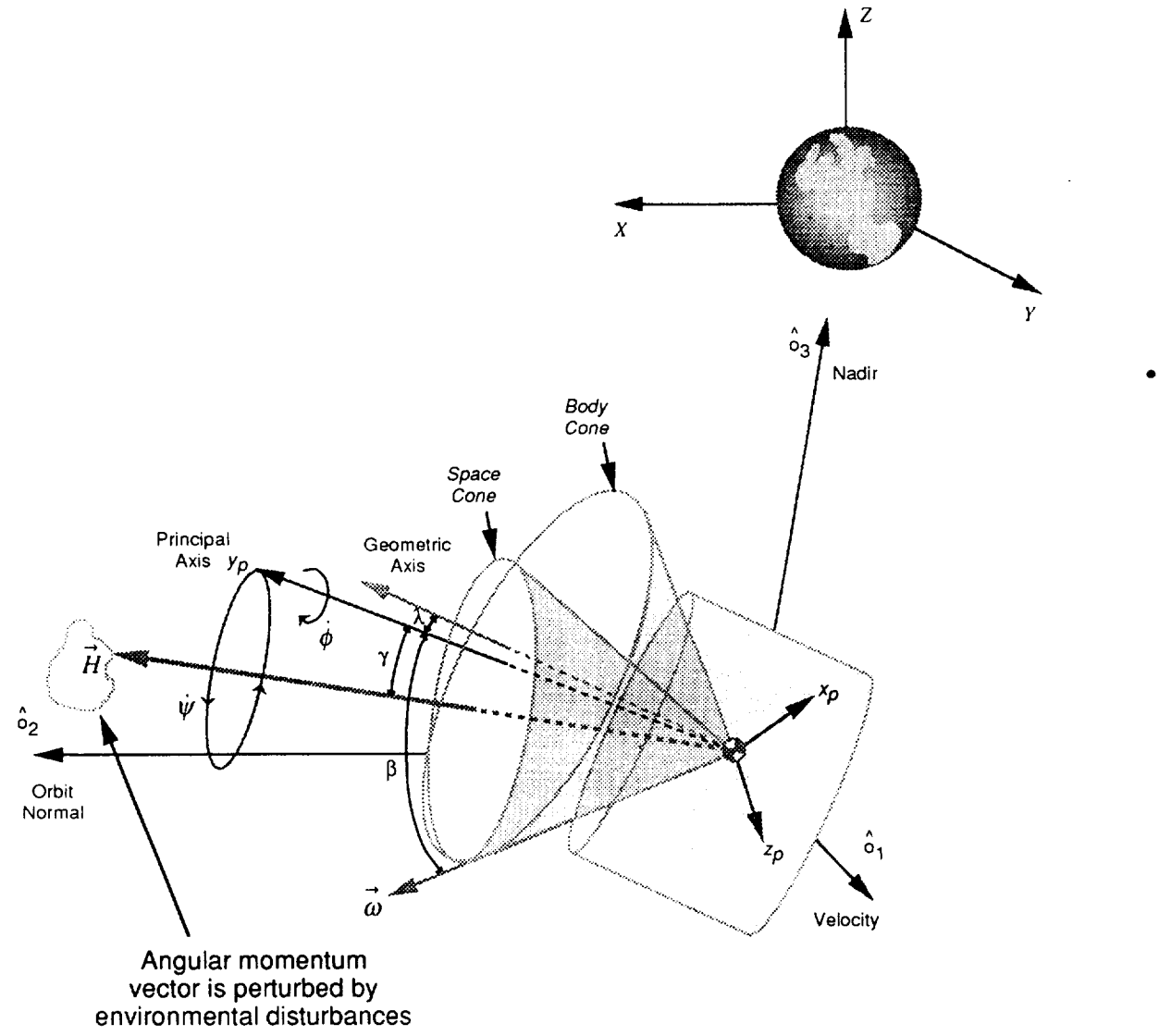

Figure 12. Principal axis precesses around the angular momentum vector, which is perturbed by the environmental disturbances.

As shown in figure 13, two options were considered for nutation damper orientation: circumferentially mounted dampers and meridially oriented dampers. Equations of motion for both orientations were derived, and linearized systems of equations were determined. The circumferentially mounted dampers provide damping through nonlinear terms in the equations of motion, and are in general more suitable for spacecraft that will encounter large nutational motion.[7] Axially mounted dampers are more effective for small nutation angles, and affect the spacecraft motion directly through the linear terms. Since the largest nutation angle that MI will experience occurs at launch vehicle separation, and it will be less than 10° using OSC's estimates, the meridially mounted dampers were selected.

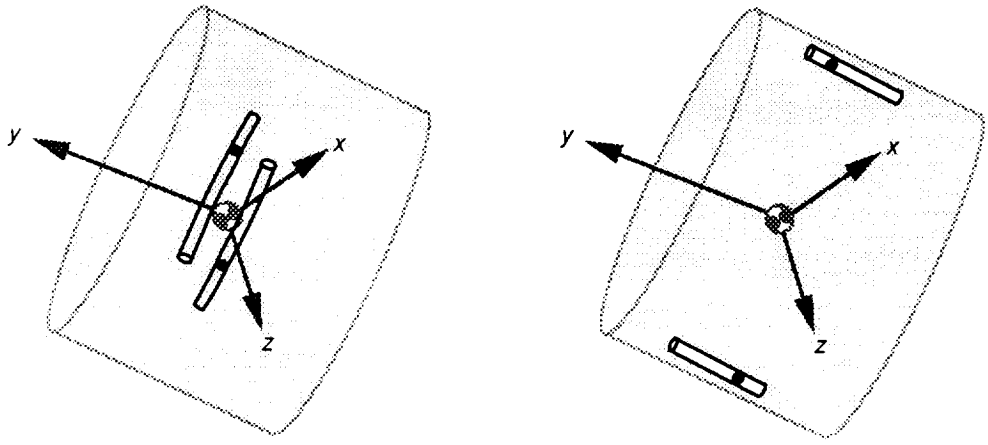

(a) Circumferential dampers (b) Meridial dampers

Figure 13. Options for damper orientation.

To demonstrate damper performance, the two meridially mounted dampers were modeled as axial spring-mass-dampers located at $\vec{\mathbf{b}}_1 = b_{1x}\hat{\mathbf{i}} + b_{1z}\hat{\mathbf{k}}$ and $\vec{\mathbf{b}}_2 = b_{2x}\hat{\mathbf{i}} + b_{2z}\hat{\mathbf{k}}$ with respect to the spacecraft center-of-mass, as shown in figure 13b. The damper mass displacements are represented by ξ_1 and ξ_2 along the spacecraft spin axis. The equations of motion are linearized for small angles α_1 and α_3 about the two transverse axes, and the spin rate ν about the y-axis is treated as a constant. For damper masses m_d, damping constants c_d and stiffness constants k_d, the following equations govern the linearized motion:

$$\mathbf{M}\ddot{q} + (\mathbf{G} + \mathbf{D})\dot{q} + \mathbf{K}q = 0 \ , \tag{1}$$

where the state vector $q = \{\alpha_1 \quad \alpha_3 \quad \xi_1 \quad \xi_2\}^T$. The mass matrix is:

$$\mathbf{M} = \begin{bmatrix} I_1 & 0 & -m_d b_{1z} & -m_d b_{2z} \\ 0 & I_3 & m_d b_{1x} & m_d b_{2x} \\ -m_d b_{1z} & m_d b_{1x} & m_d - m_d^2/m & m_d^2/m \\ -m_d b_{2z} & m_d b_{2x} & m_d^2/m & m_d - m_d^2/m \end{bmatrix} , \tag{2}$$

the gyroscopic matrix is:

$$G = \nu \begin{bmatrix} 0 & I_1+I_3-I_2 & 0 & 0 \\ -(I_1+I_3-I_2) & 0 & 0 & 0 \\ 0 & 0 & 0 & 0 \\ 0 & 0 & 0 & 0 \end{bmatrix}, \tag{3}$$

the damping matrix is $\mathbf{D} = \text{diag}\{0 \quad 0 \quad c_d \quad c_d\}$, and the stiffness matrix is:

$$\mathbf{K} = \nu^2 \begin{bmatrix} I_2-I_3 & 0 & -m_d b_{1z} & -m_d b_{2z} \\ 0 & I_2-I_1 & m_d b_{1x} & m_d b_{2x} \\ -m_d b_{1z} & m_d b_{1x} & k_d/\nu^2 & 0 \\ -m_d b_{2z} & m_d b_{2x} & 0 & k_d/\nu^2 \end{bmatrix}. \tag{4}$$

The spacecraft principal moments-of-inertia are I_1, I_2, and I_3, and the total spacecraft mass is m.

The linearized equations of motion were used to tune the damper performance. This analysis used spacecraft inertias and mass with an added 30 percent contingency, I_1 = 75.1 kg m^2, I_2 = 81.0 kg m^2, and I_3 = 73.8 kg m^2, and a mass of 285 kg. The dampers were tuned using a root-locus technique in which the spring constant and damping constant were varied, using a damper mass of 0.5 kg. A sample of the root-locus is shown in figure 14, for a damping constant of 0.03 kg/s and the stiffness constant varying from 0.3 kg/s^2 down to 0.032 kg/s^2. The root locus to the far left splits at k_d = 0.07 kg/s^2, which was the value selected for use in the simulations. As the stiffness constant is decreased further, the root locus to the right converges to the real axis and then splits and becomes unstable.

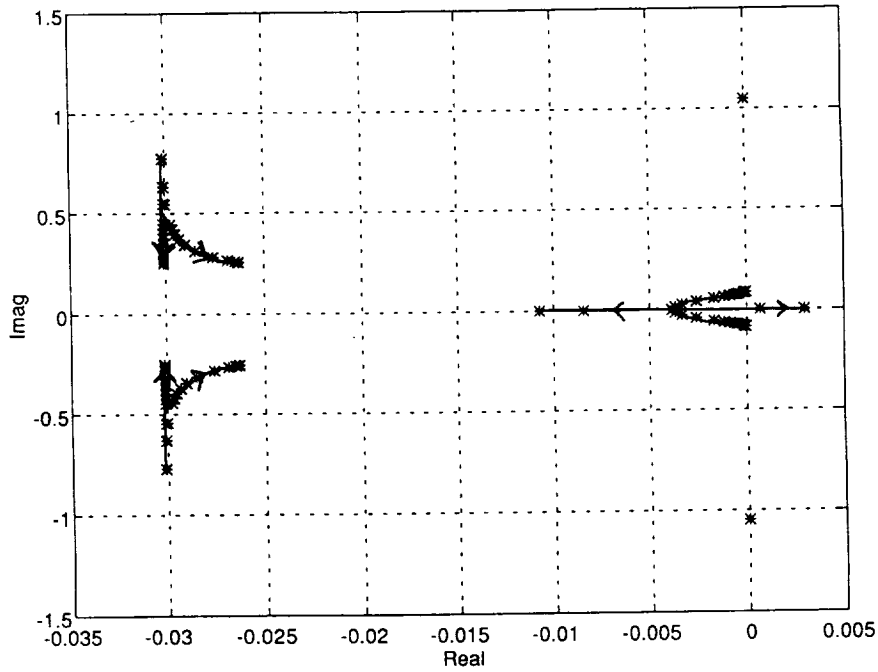

Figure 14. Root locus for damper tuning. The arrows indicate the locus direction for decreasing values of the stiffness constant k_d.

The nonlinear equations that govern rotational motion are:

$$\dot{\vec{\mathbf{h}}} = -\vec{\omega}\times\vec{\mathbf{h}} - \vec{\mathbf{v}}\times\vec{\mathbf{p}} + \vec{\mathbf{g}} \ ,$$

$$\dot{p}_{n1} = m_d \vec{\omega}^{\mathrm{T}} \hat{\mathbf{n}}\times(\vec{\mathbf{v}} - \vec{\mathbf{r}}_{d1}\times\vec{\omega}) - c_d\dot{\xi}_1 - k_d\xi_1 \ , \tag{5}$$

$$\dot{p}_{n2} = m_d \vec{\omega}^{\mathrm{T}} \hat{\mathbf{n}}\times(\vec{\mathbf{v}} - \vec{\mathbf{r}}_{d2}\times\vec{\omega}) - c_d\dot{\xi}_2 - k_d\xi_2 \ ,$$

where,

$$\vec{\mathbf{h}} = \vec{\mathbf{c}}\times\vec{\mathbf{v}} + \mathbf{J}\vec{\omega} + m_d\dot{\xi}_1\vec{\mathbf{b}}_1\times\hat{\mathbf{j}} + m_d\dot{\xi}_2\vec{\mathbf{b}}_2\times\hat{\mathbf{j}} \ ,$$

$$p_{n1} = m_d(\mathbf{v}_2 - \hat{\mathbf{n}}^{\mathrm{T}}\vec{\mathbf{b}}_1\times\vec{\omega} + \dot{\xi}_1) \ , \tag{6}$$

$$p_{n2} = m_d(\mathbf{v}_2 - \hat{\mathbf{n}}^{\mathrm{T}}\vec{\mathbf{b}}_2\times\vec{\omega} + \dot{\xi}_2) \ .$$

The vector $\vec{\mathbf{v}}$ is the spacecraft velocity in body coordinates, $\vec{\mathbf{p}}$ is the system linear momentum, p_{n1} and p_{n2} are the damper linear moments, and $\vec{\omega}$ is the spacecraft angular velocity. The vector $\vec{\mathbf{g}}$ is the external torque on the spacecraft. The unit vector $\hat{\mathbf{n}}$ is the direction of motion for the damper masses, which in this case is along the spacecraft spin axis $\hat{\mathbf{j}}$, and $\vec{\mathbf{r}}_{di} = \vec{\mathbf{b}}_i + \xi_i\hat{\mathbf{n}}$ are the vectors locating the damper masses with respect to the center-of-mass. The system inertia matrix **J** is:

$$\mathbf{J} = \mathbf{I} + m_d\xi_1\left\{2\vec{\mathbf{b}}_1^{\dagger}\hat{\mathbf{n}}\mathbf{1} - \vec{\mathbf{b}}_1\hat{\mathbf{n}}^{\mathrm{T}} - \hat{\mathbf{n}}\vec{\mathbf{b}}_1^{\dagger}\right\} + m_d\xi_2\left\{2\vec{\mathbf{b}}_2^{\dagger}\hat{\mathbf{n}}\mathbf{1} - \vec{\mathbf{b}}_2\hat{\mathbf{n}}^{\mathrm{T}} - \hat{\mathbf{n}}\vec{\mathbf{b}}_2^{\dagger}\right\} \ . \tag{7}$$

The rotational equations are coupled to the translational equations of motion that define the spacecraft orbit, forming an 8 degree-of-freedom system. Gravity-gradient torques, solar radiation pressure forces and torques, and aerodynamic forces and torques are modeled in the simulation. All simulation results assume a 4,800 km × 7 R_e orbit.

As indicated in table 3, the predominant environmental torque on MI is that due to solar radiation pressure. This disturbance is computed in the simulation assuming the spacecraft has 12 sides, covered with solar arrays, and two end plates. The force on each surface is determined using the geometric centroid of each surface as its center-of-pressure. The net torque about the spacecraft center-of-mass is computed assuming that the center-of-mass is slightly offset from the spacecraft geometric center. To obtain a conservative estimate for this disturbance torque, the reflected solar radiation is assumed to be completely specular with a reflection fraction of 0.02 for the solar arrays. The end plates are assumed to be totally reflective. A similar conservative model is used to estimate the aerodynamic torques on MI, but these are still negligible because of the high orbit altitudes.

The system response to worst-case tip-off conditions from the launch vehicle was simulated. The initial attitude errors were 2° in each axis, with an initial tip-off rate of 3°/s in each transverse axis. The beta angle was 0°. The nutation angle between the vehicle principal axis and the angular

momentum vector is shown in figure 15, with the corresponding damper mass motion shown in figures 16 and 17. The dampers decrease the wobble to less than 0.025° in approximately 2 h.

The launch vehicle tip-off rates not only produce alignment errors between the vehicle principal axis and the angular momentum vector, but also between the angular momentum vector and the orbit normal. Although the dampers remove the errors between the principal axis and the angular momentum vector, the magnetic torquer is needed to align the angular momentum vector with the orbit normal. The worst-case launch vehicle separation conditions produce an error between the spacecraft spin axis and the orbit normal that is equal to 3.5° after 2 h, as shown in figure 18.

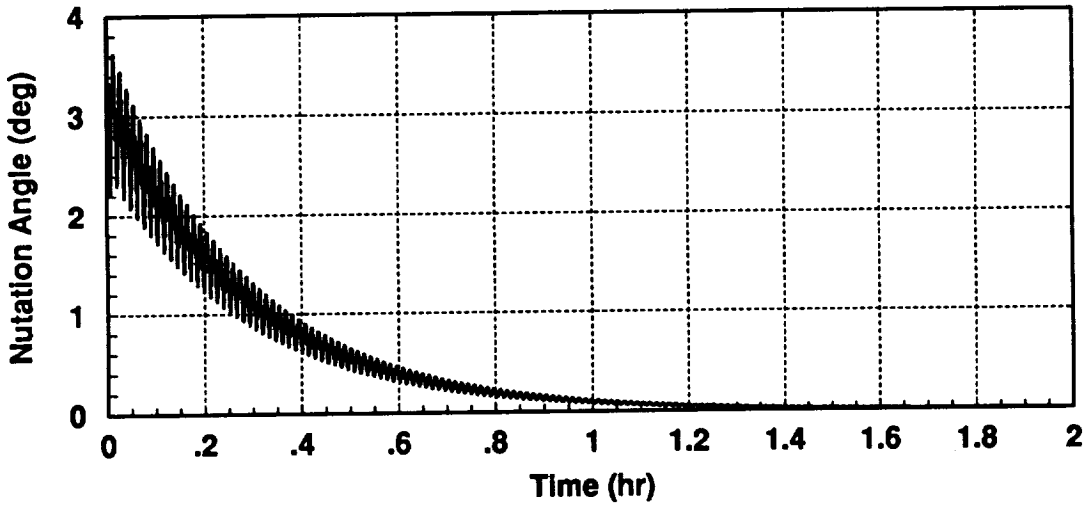

Figure 15. Nutation angle after worst-case launch vehicle tip-off conditions.

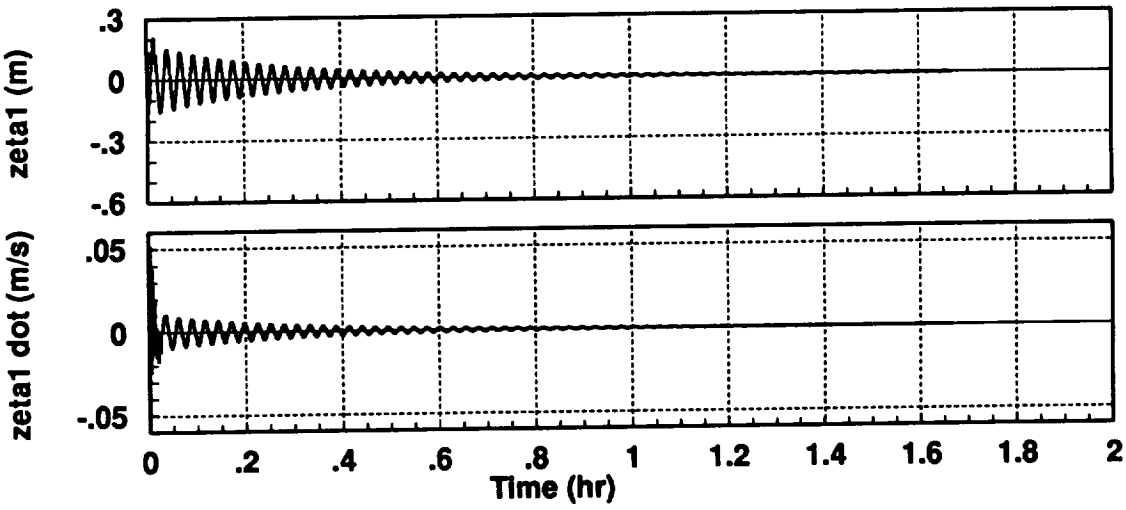

Figure 16. Position and velocity for damper mass 1.

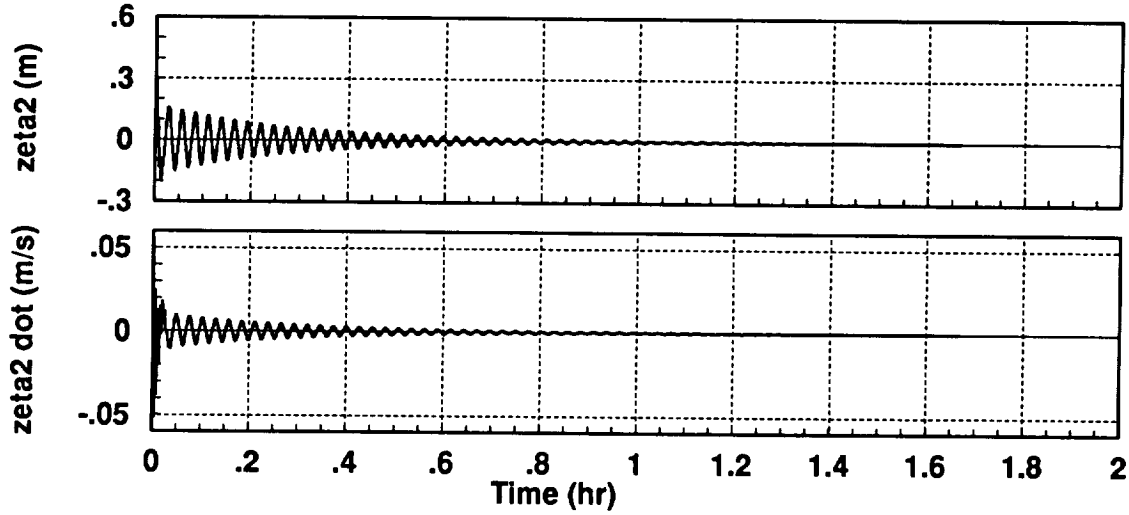

Figure 17. Position and velocity for damper mass 2.

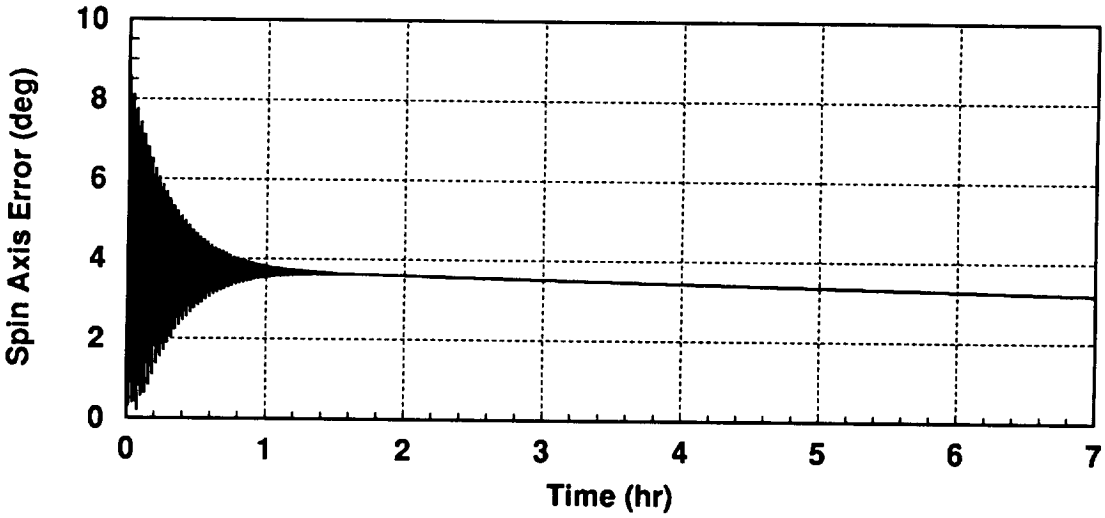

Figure 18. Angle between the spacecraft spin axis and the orbit normal after worst-case launch vehicle tip-off conditions.

As previously noted, the largest environmental disturbance torque is due to solar radiation pressure. It is a maximum when β is 45° and a minimum when β is 0°. Figures 19, 20, and 21 show the magnitude of the solar radiation pressure, gravity gradient, and aerodynamic torques over half an orbit for $\beta = 45°$, from perigee to apogee. Figure 22 shows the vector sum of these torques resolved into spacecraft axes.

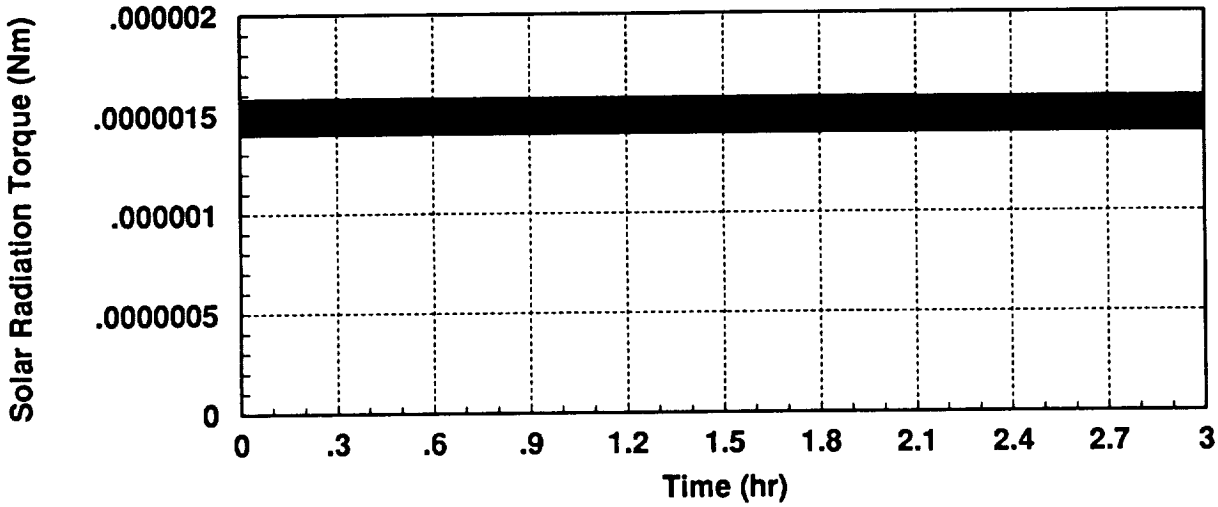

Figure 19. Magnitude of the solar radiation torque for $\beta = 45^{\circ}$.

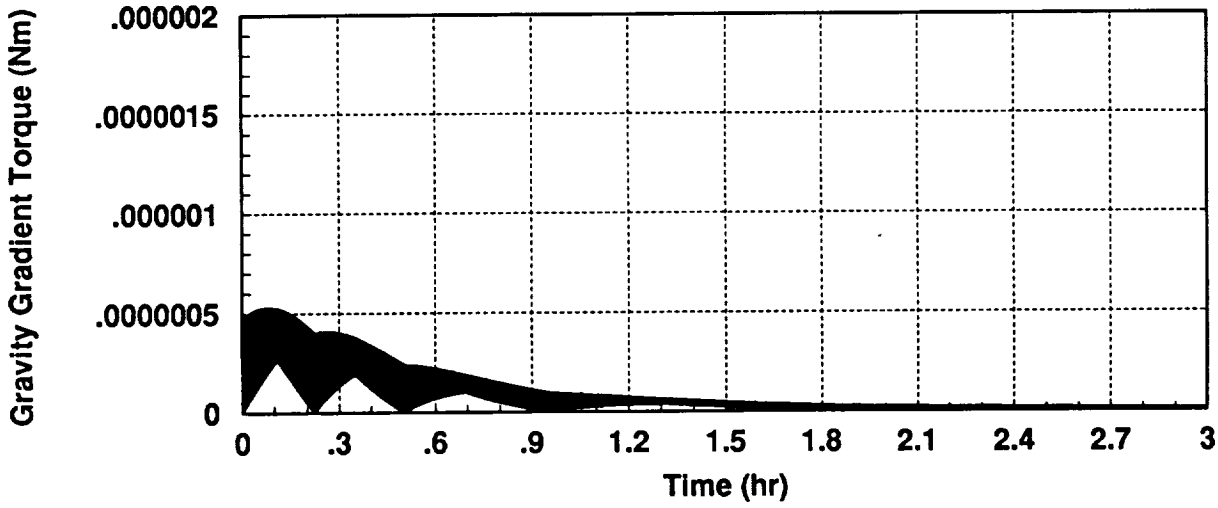

Figure 20. Magnitude of the gravity-gradient torque for $\beta = 45^{\circ}$.

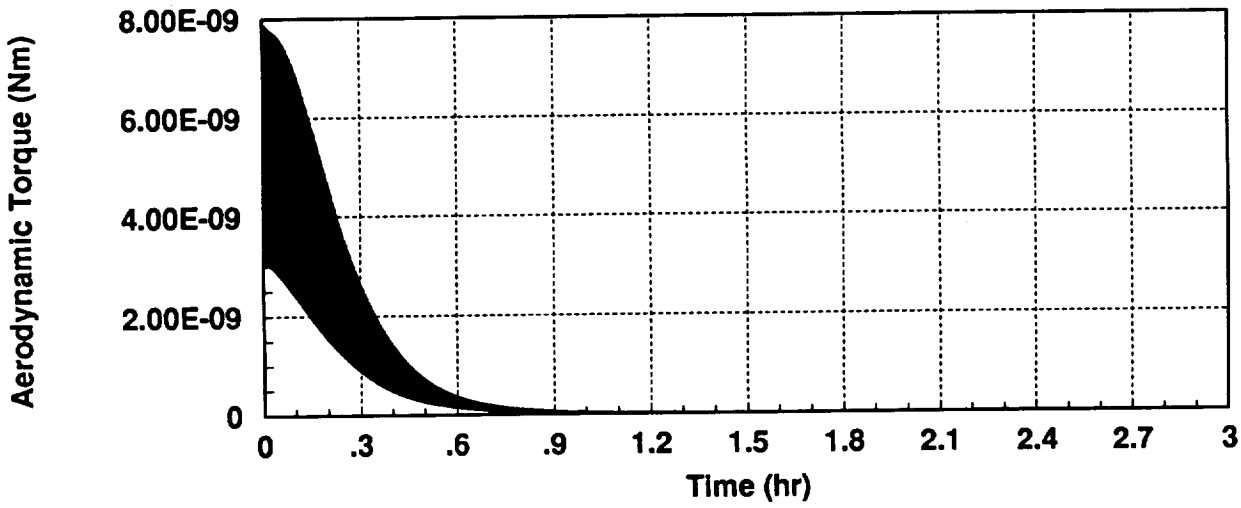

Figure 21. Magnitude of the aerodynamic torque for $\beta = 45^{\circ}$.

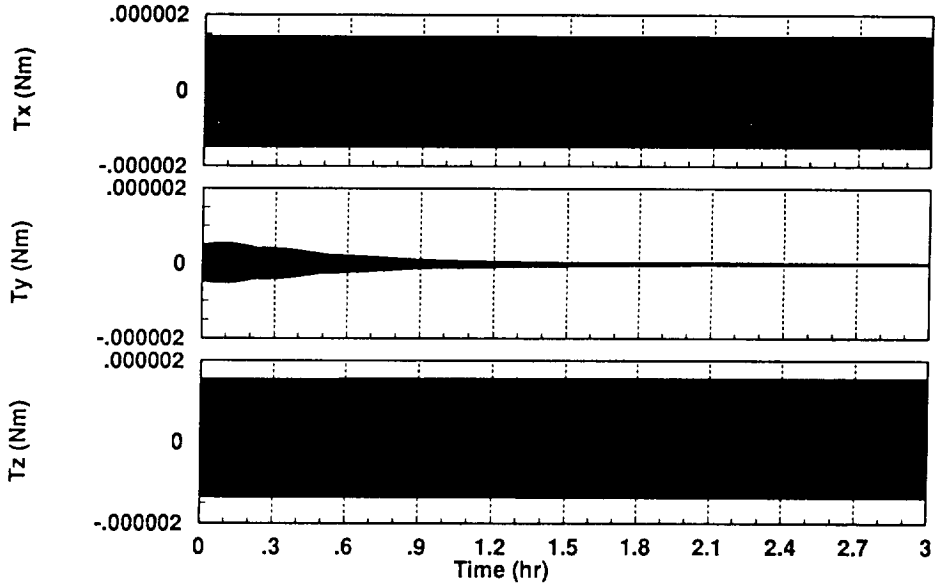

Figure 22. Environmental disturbance torques in spacecraft axes, for $\beta = 45°$.

The system response to these disturbance torques was simulated over a quarter of an orbit starting at perigee, for $\beta = 45°$ and a 4,800 km $\times$ 7 R_e orbit. Initially, the spacecraft spin axis was aligned with the orbit normal, the spin rate was 10 rpm, and the angular rates in the other two axes were zero. Figure 23 shows the angle in arcsec between the spacecraft spin axis and the orbit normal. It is well below 1° and the motion of the spin axis is well below 0.025° over any 60 s period. The corresponding angular velocity components along the two transverse axes are shown in figures 24 and 25, with the corresponding Euler angles in arcsec plotted in figures 26 and 27. The spin rate over two full orbits is shown in figure 28, and its deviation from 10 rpm is plotted in figure 29. Perturbations to the spin rate are greatest at perigee when the gravity gradient torques are maximum. Figure 29 shows that the spin rate decay due to gravity gradient, solar radiation pressure, and aerodynamic torques is expected to be 4×10^{-8} rpm per orbit. This corresponds to a negligible amount over the 2 year mission. Hence, the only significant loss in spin rate is that due to eddy current losses in the spacecraft aluminum structure, which could be about 0.5 rpm over 2 years, as shown in table 3. On the other hand, if it turns out the spin rate decay is much greater than anticipated, the magnetic torquing system for adjusting the spin rate can be employed as required to maintain it within the required range of 10±5 rpm.

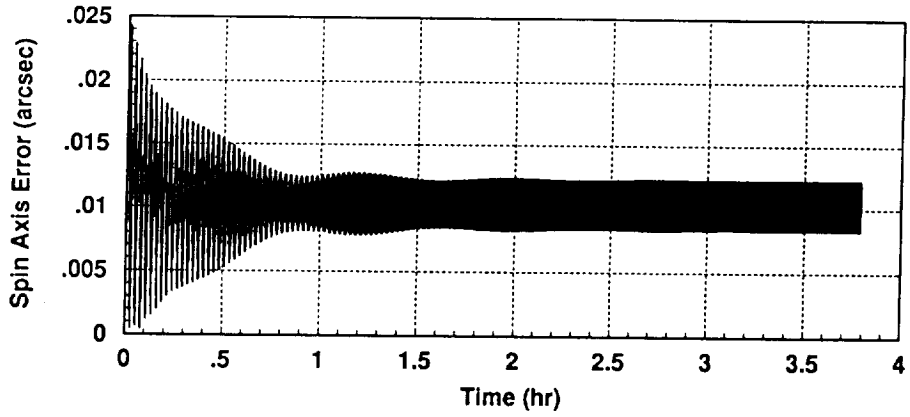

Figure 23. Angle between the spacecraft spin axis and the orbit normal, due to environmental disturbances when $\beta = 45°$.

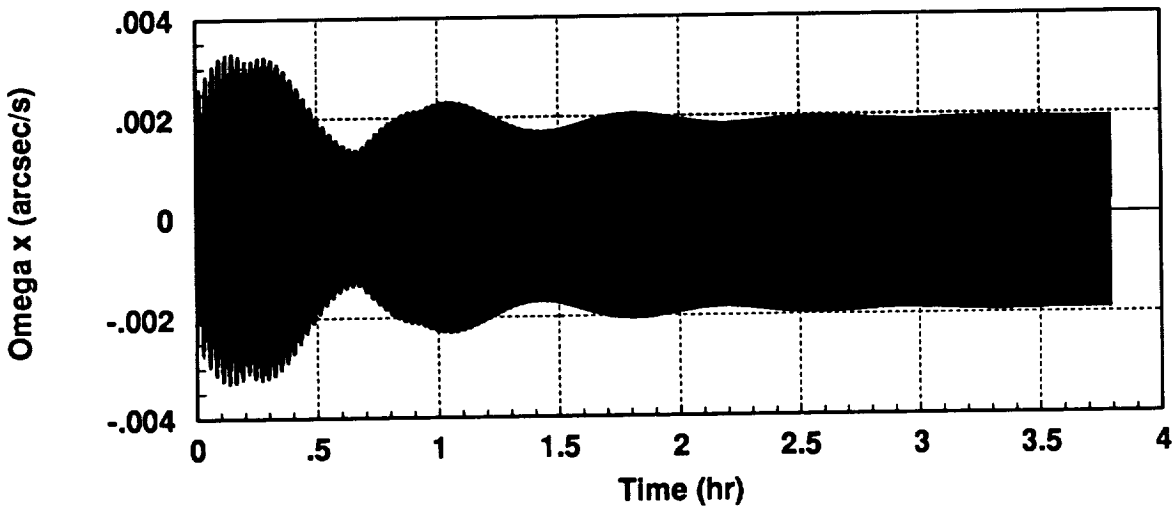

Figure 24. Angular velocity component along the spacecraft x-axis, for $\beta = 45°$.

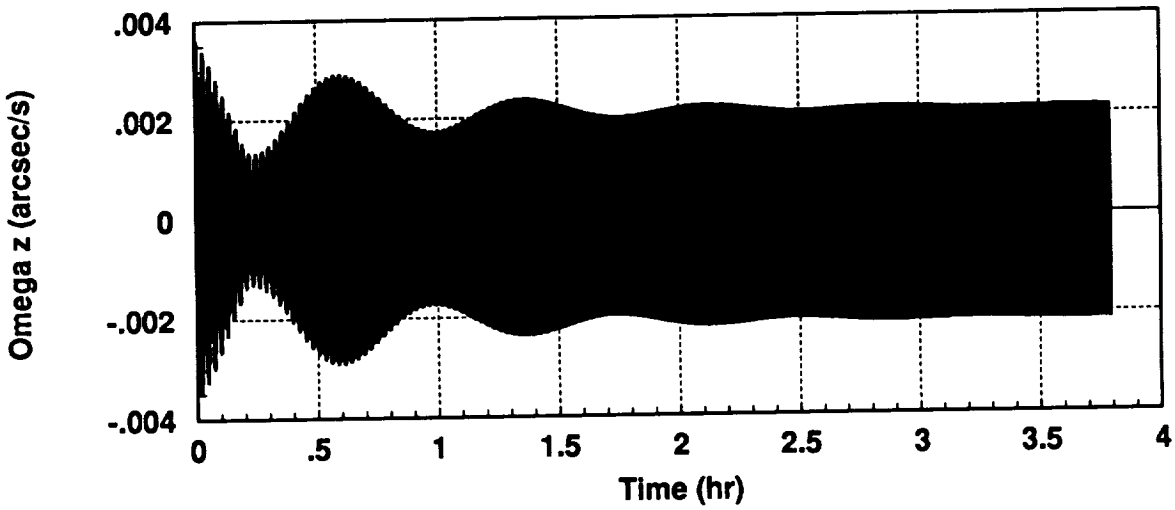

Figure 25. Angular velocity component along the spacecraft z-axis, for $\beta = 45°$.

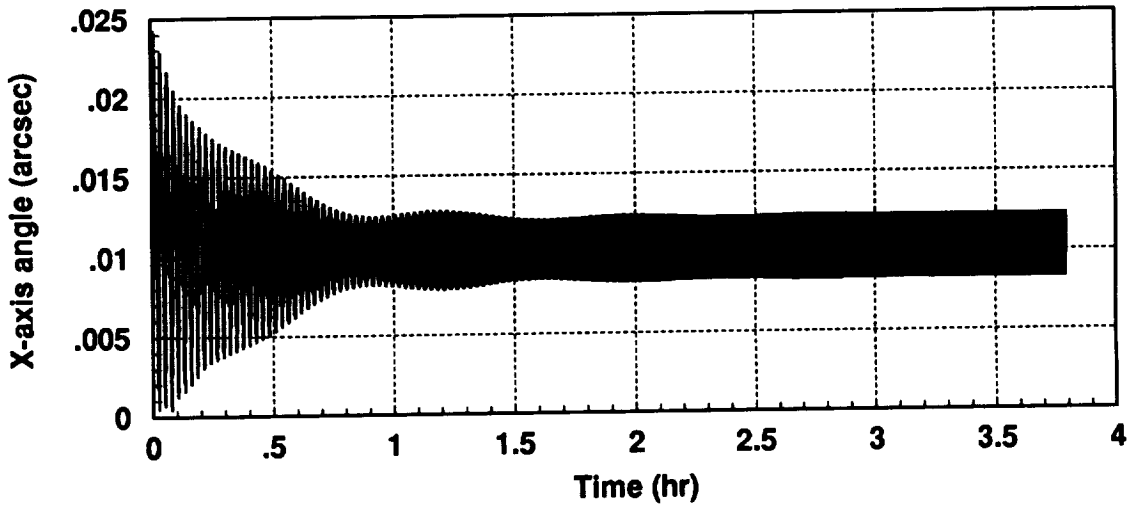

Figure 26. X-axis angle, of the 2-1-3 Euler angles from an inertial frame aligned with the orbit to the spacecraft-fixed frame.

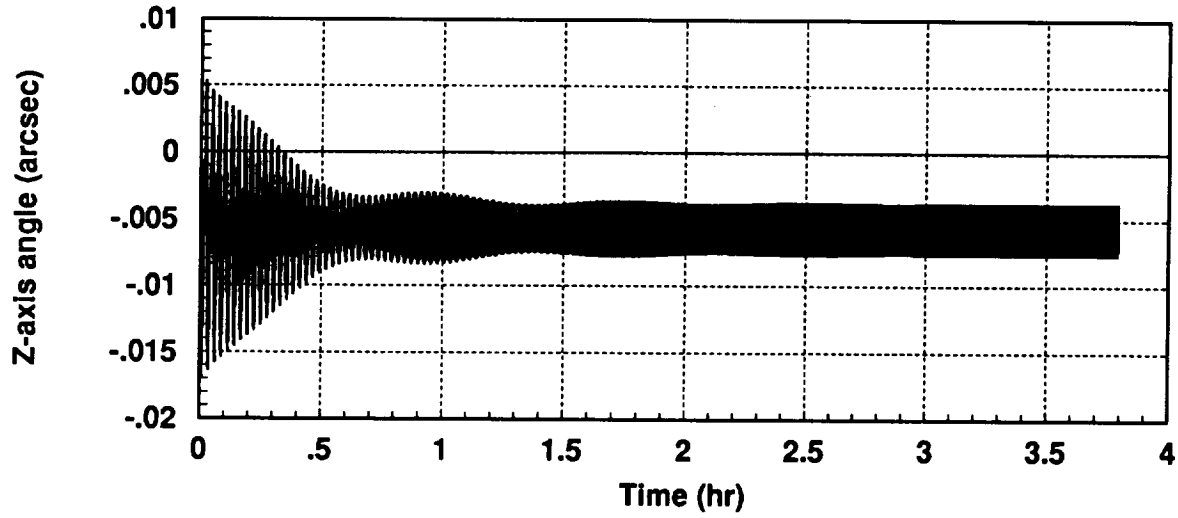

Figure 27. Z-axis angle, of the 2-1-3 Euler angles from an inertial frame aligned with the orbit to the spacecraft-fixed frame.

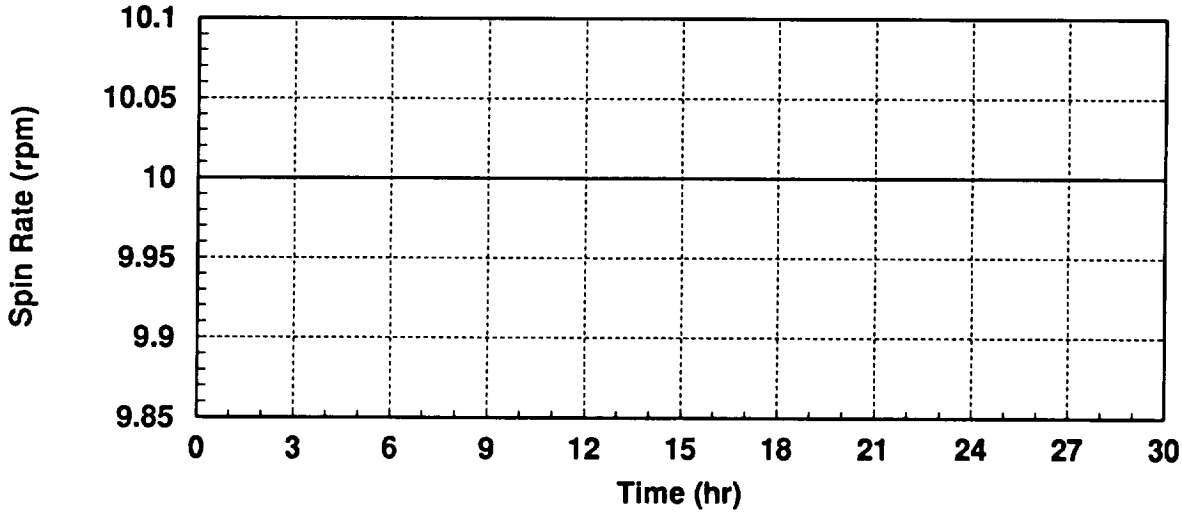

Figure 28. Spacecraft spin rate over two orbits, for $\beta = 45°$.

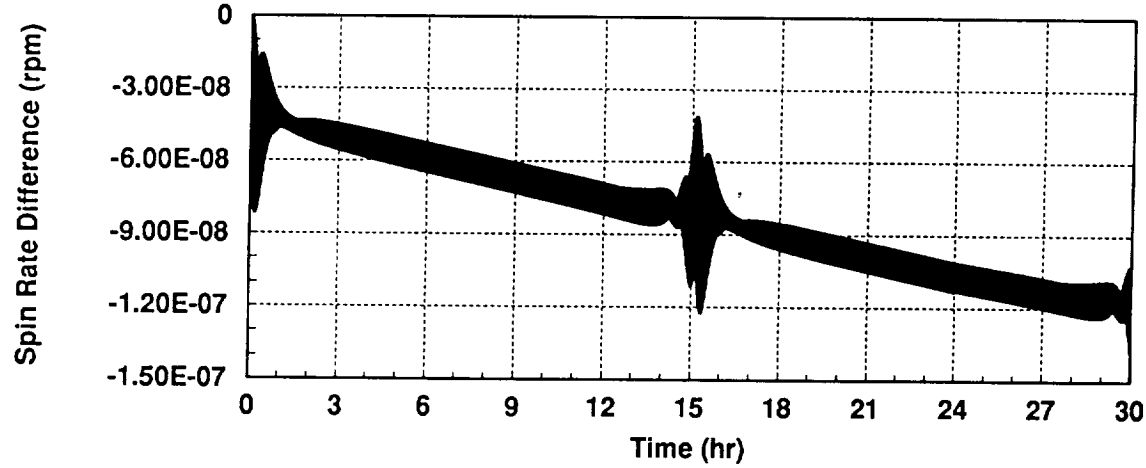

Figure 29. Change in spin rate over two orbits, for $\beta = 45°$.

VI. CONCLUDING REMARKS

This paper has presented a conceptual design for the attitude control and determination (ACAD) system for the Magnetosphere Imager (MI) spacecraft. The proposed system is low-power, low-mass, very simple conceptually, and highly passive. No onboard ACAD software algorithms are required. The proposed design is consistent with the overall MI design philosophy, which is faster-better-cheaper. Still, the proposed ACAD system is extremely robust and can handle a number of unexpected, adverse situations on orbit without impacting the MI mission as a whole.

REFERENCES

1. Mullins, L.: "Geomagnetic Field Calculations Around the Magnetosphere Imager Orbit." NASA Marshall Space Flight Center internal memo No. EL58 (42-94), June 15, 1994.

2. Mullins, L.: "UV Stars Available for Inner Magnetospheric Imager (IMI) Star Trackers." NASA Marshall Space Flight Center internal memo No. EL58 (31-94), April 18, 1994.

3. Singer, S.F.: "Torques and Attitude Sensing in Earth Satellites." Academic Press, New York, 1964, pp. 159–174.

4. Woodard, D.: "Magnetic Moments and Torques on the AAP Cluster Configuration." Internal memorandum, Bellcomm, Washington, DC, 1967.

5. Smith, G.: "Effects of Magnetically Induced Eddy-Current Torques on Spin Motions of an Earth Satellite." NASA TN D-2198, NASA Langley Research Center, Hampton, VA, 1965.

6. Smith, G.: "A Theoretical Study of the Torques Induced by a Magnetic Field on Rotating Cylinders and Spinning Thin-Wall Cones, Cone Frustums, and General Bodies of Revolution." NASA TR R-129, NASA Langley Research Center, Hampton, VA, 1965.

7. Hughes, P.: "Spacecraft Attitude Dynamics." Wiley and Sons, New York, 1986, pp. 392–393.

☆ U.S. GOVERNMENT PRINTING OFFICE-1995-633-109 /20047

REPORT DOCUMENTATION PAGE

Form Approved
OMB No. 0704-0188

1. AGENCY USE ONLY (Leave blank)	2. REPORT DATE	3. REPORT TYPE AND DATES COVERED
	May 1995	Technical Paper

4. TITLE AND SUBTITLE
A Conceptual Design for the Attitude Control and Determination System for the Magnetosphere Imager Spacecraft

5. FUNDING NUMBERS

6. AUTHOR(S)
M.E. Polites and C.K. Carrington

7. PERFORMING ORGANIZATION NAME(S) AND ADDRESS(ES)
George C. Marshall Space Flight Center
Marshall Space Flight Center, Alabama 35812

8. PERFORMING ORGANIZATION REPORT NUMBER
M-784

9. SPONSORING/MONITORING AGENCY NAME(S) AND ADDRESS(ES)
National Aeronautics and Space Administration
Washington, DC 20546-0001

10. SPONSORING/MONITORING AGENCY REPORT NUMBER
NASA TP-3560

11. SUPPLEMENTARY NOTES
Prepared by Structures and Dynamics Laboratory, Science and Engineering Directorate and the Preliminary Design Office, Program Development

12a. DISTRIBUTION/AVAILABILITY STATEMENT
Unclassified–Unlimited
Subject Category 18

12b. DISTRIBUTION CODE

13. ABSTRACT *(Maximum 200 words)*

This paper presents a conceptual design for the attitude control and determination (ACAD) system for the Magnetosphere Imager (MI) spacecraft. The MI is a small spin-stabilized spacecraft that has been proposed for launch on a Taurus-S expendable launch vehicle into a highly-elliptical polar Earth orbit. Presently, launch is projected for 1999. The paper describes the MI mission and ACAD requirements and then proposes an ACAD system for meeting these requirements. The proposed design is low-power, low-mass, very simple conceptually, highly passive, and consistent with the overall MI design philosophy, which is faster-better-cheaper. Still, the MI ACAD system is extremely robust and can handle a number of unexpected, adverse situations on orbit without impacting the mission as a whole. Simulation results are presented that support the soundness of the design approach.

14. SUBJECT TERMS
Attitude Control, Attitude Determination, Conceptual Design, Earth Orbiting, Horizon Crossing Indicators, Magnetic Torquers, Magnetometers, Nutation Dampers, Satellite, Spacecraft, Spin Stabilized, Sun Sensors

15. NUMBER OF PAGES
29

16. PRICE CODE
A03

17. SECURITY CLASSIFICATION OF REPORT	18. SECURITY CLASSIFICATION OF THIS PAGE	19. SECURITY CLASSIFICATION OF ABSTRACT	20. LIMITATION OF ABSTRACT
Unclassified	Unclassified	Unclassified	Unlimited